Original Article - Basic/Translational Research

Investig Clin Urol 2021;62:100-110.
https://doi.org/10.4111/icu.20200272
pISSN 2466-0493 • eISSN 2466-054X

INVESTIGATIVE AND CLINICAL UROLOGY
ICUROLOGY

Transcriptional profiling of mouse cavernous pericytes under high-glucose conditions: Implications for diabetic angiopathy

Guo Nan Yin[1,*], Jitao Wu[2,*], Yuanshan Cui[2], Chunhua Lin[2], Lei Shi[2], Zhen-Li Gao[2], Jun-Kyu Suh[1], Ji-Kan Ryu[1], Hai-Rong Jin[2]

[1]Department of Urology, National Research Center for Sexual Medicine, Inha University School of Medicine, Incheon, Korea, [2]Department of Urology, Yantai Yuhuangding Hospital Affiliated to Medical College of Qingdao University, Yantai, Shandong, China

Purpose: Penile erection requires integrative interactions between vascular endothelial cells, pericytes, smooth muscle cells, and autonomic nerves. Furthermore, the importance of the role played by pericytes in the pathogenesis of angiopathy has only recently been appreciated. However, global gene expression in pericytes in diabetes mellitus-induced erectile dysfunction (DMED) remains unclear. We aimed to identify potential target genes related to DMED in mouse cavernous pericytes (MCPs).

Materials and Methods: Mouse cavernous tissue was allowed to settle under gravity in collagen I-coated dishes, and sprouted cells were subcultivated for experiments. To imitate diabetic conditions, MCPs were treated with normal-glucose (NG, 5 mM) or high-glucose (HG, 30 mM) media for 3 days. Microarray technology was used to evaluate gene expression profiles, and RT-PCR was used to validate sequencing data. Histological examinations and Western blot were used to validate final selected target genes related to DMED.

Results: Decreased tube formation and increased apoptosis were detected in MCPs exposed to the HG condition. As shown by microarray analysis, the gene expression profiles of MCPs exposed to the NG or HG condition differed. A total of 2,523 genes with significantly altered expression were classified into 15 major gene categories. After further screening based on gene expression and RT-PCR and histologic results, we found that Hebp1 gene expression was significantly diminished under the HG condition and in DM mice.

Conclusions: This gene profiling study provides new potential targets responsible for diabetes in MCPs. Validation studies suggest that Hebp1 may be a suitable biomarker for DMED.

Keywords: Diabetes mellitus; Erectile dysfunction; Gene expression; Microarray analysis

Received: 14 June, 2020 • **Revised:** 13 July, 2020 • **Accepted:** 21 July, 2020 • **Published online:** 24 November, 2020

Corresponding Authors:
Hai-Rong Jin https://orcid.org/0000-0002-0476-1531
Department of Urology, Yantai Yuhuangding Hospital Affiliated to Medical College of Qingdao University, 20 Yuhuangding East Road, Yantai, Shandong, 264000, China
TEL: +86-133-6535-8707, FAX: +86-535-669-5579, E-mail: jhr2006@163.com
Ji-Kan Ryu https://orcid.org/0000-0003-0025-6025
Department of Urology, National Research Center for Sexual Medicine, Inha University School of Medicine, 7-206, 3rd ST, Shinheung-dong, Jung-gu, Incheon 22332, Korea
TEL: +82-32-890-3505, FAX: +82-32-890-3099, E-mail: rjk0929@inha.ac.kr
*These authors contributed equally to this study and should be considered co-first authors.

INTRODUCTION

Diabetes mellitus (DM) causes erectile dysfunction (ED) with severe angiopathy, which is the main reason for the reduced efficacy of phosphodiesterase-5 (PDE5) inhibitors in DM [1,2]. Several studies have presented gene expression profiles of cavernosum tissue and cavernous endothelial cells in diabetes-induced ED [3-5], but the genetic mechanisms responsible have yet to be elucidated and more molecular candidates are needed.

Pericytes are multifunctional mural cells that surround endothelial cells and support vascular development and homeostasis [6-8]. Accumulating evidence shows that pericytes play important roles in vascular contractility and constitute a reservoir of mesenchymal stem cells [9]. In mouse cavernosum tissue, we found that the distribution of pericytes protrudes more into in the microvessels of the subtunical area than in the cavernous sinusoids. As we know, oxidized low-density lipoprotein (LDL) mediates oxidative stress and can induce pericyte apoptosis and diabetic retinopathy [10,11]. We recently observed that a loss of pericytes increases the leakage of oxidized LDL in mice with diabetes-induced ED, which may hinder the expansion of erectile tissue by inducing cavernous inflammation and fibrosis *in vivo* and *in vitro* [1]. Restoration of the cavernous pericyte content by injection of hepatocyte growth factor significantly decreases cavernous vascular permeability. However, the detailed functional roles of pericytes in penile erection are still largely unknown.

Physiologic and pathologic gene expression profiling provides a means of understanding the molecular mechanisms underlying diabetes-induced ED and of identifying novel treatment targets. In the present study, we performed a microarray assay on mouse cavernous pericytes (MCPs) exposed to normal-glucose (NG, 5 mM) or high-glucose (HG, 30 mM) conditions, which were used to mimic diabetes-induced angiopathy, and we identified genes differentially induced in MCPs under these conditions. After screening for significantly altered genes, *Hebp1* was chosen as a potential novel therapeutic candidate for diabetes-induced ED.

MATERIALS AND METHODS

1. Ethical statement and animals

Eight-week-old adult male C57BL/6J mice were used in this study (5 for MCP characterization, 10 for the *in vitro* functional study, 6 for microarray assays, 10 for RT-PCR validation of the microarray results, and 12 for the diabetes study). All animal experiments were approved by the Institutional Animal Care and Use Committee of the Inha University (approval number: INHA 170112-475).

Diabetes was induced by injecting multiple low doses of streptozotocin (STZ, S0130; Sigma-Aldrich, St. Louis, MO, USA) intraperitoneally (50 mg/kg body weight per day in 0.1 M citrate buffer, pH 4.5) for 5 consecutive days. Eight weeks after STZ administration, mice were anesthetized with intramuscular injections of ketamine (100 mg/kg) and xylazine (5 mg/kg) and placed supine on a thermoregulated surgical table as described previously [12,13].

2. Primary culture of MCPs

Primary cultures of MCPs were performed as previously described [14-16]. Briefly, penis tissues were harvested and placed in sterile vials containing Hank's balanced salt solution (HBSS; Gibco, Carlsbad, CA, USA). Urethras and dorsal neurovascular bundles were removed and only corpus cavernosum tissues were washed three times with phosphate-buffered saline (PBS). Corpus cavernosum tissues were cut into small pieces (1–2 mm) and allowed to settle into collagen I-coated 35-mm cell culture dishes containing a 300-μL complement of Dulbecco's modified Eagle Medium (DMEM, Gibco) in a 5% CO_2 atmosphere at 37°C. After 20 minutes, 900 μL of complement medium (20% fetal bovine serum, 1% penicillin/streptomycin, and 10 nM human pigment epithelium-derived factor [MFCD03792528, Sigma-Aldrich]) was added and tissues were incubated in 5% CO_2 at 37°C. The medium was changed every 2 days and after culture for 2 weeks, only sprouting cells were subcultured to dishes coated with collagen I (#5005; Advanced BioMatrix, San Diego, CA, USA). MCPs at passages 2 or 3 were used for experiments.

To determine cell types, cells were stained with antibodies against NG2 (a pericyte marker, AB5320; Millipore, Temecula, CA, USA; 1:50), CD31 (an endothelial cell marker, MAB1398Z; Millipore; 1:50), PDGFRβ (a pericyte marker, SC-1627; Santa Cruz Biotechnology, Santa Cruz, CA, USA; 1:50), smooth muscle α-actin (smooth muscle cell and pericyte marker, A2547; Sigma-Aldrich; 1:200), or DAPI (a nuclear marker, H-1500; Vector Laboratories, Inc., Burlingame, CA, USA). Digital images were obtained using a confocal fluorescence microscope (K1-Fluo; Nanoscope Systems, Inc., Daejeon, Korea).

3. Tube formation assay

Tube formation assays were performed to evaluate angiogenesis by cultured MCPs in the NG (5 mM, G7021, Sigma-Aldrich) or HG (30 mM) condition [10]. Briefly, about 50 μL of growth factor-reduced Matrigel (354234; Becton Dickinson, Mountain View, CA, USA) was dispensed into 96-

well culture dishes at 4℃ and allowed to gel for at least 10 minutes at 37℃. MCPs were preconditioned to NG or HG conditions for 3 days and then seeded into wells at 2×10^4 cells/well in 200 μL of DMEM. Tube formation and phase images were observed 16 hours later at 40×, and the number of master junctions was counted.

4. TUNEL assay

The TUNEL (terminal deoxynucleotidyl transferase-mediated deoxyuridine triphosphate nick end labeling) assay was used to evaluate MCP cell death in *in vivo* glucose conditions and *in vitro* diabetic conditions. The ApopTag® Fluorescein *in situ* Apoptosis Detection Kit (S7160; Chemicon, Temecula, CA, USA) was used according to the manufacturer's instructions. Apoptotic cell digital images and numbers were observed at a screen magnification of 200× using a confocal fluorescence microscope. Values are expressed per high-power field (400×). The percentage of TUNEL-positive cells in the *in vitro* study and the number of TUNEL-positive cells were evaluated.

5. cDNA microarray

The microarray study was performed on MCPs that had been treated with the NG (3 pooled samples) or HG (3 pooled samples) condition. cDNA microarray analysis was performed after 3 days of treatment. The microarray analysis was performed by E-Biogen Inc. (Seoul, Korea), as previously described [10]. For RNAs isolated from MCPs treated with the NG or HG condition, we synthesized target cRNA probes and performed hybridization using Agilent's Low RNA Input Linear Amplification kit (Agilent Technology, Santa Clara, CA, USA). Hybridized images were scanned using an Agilent DNA microarray scanner and quantified using Feature Extraction Software (Agilent Technology). Data normalization and gene selection were performed using GeneSpringGX 7.3 (Agilent Technology). Average normalized ratios were calculated by dividing average normalized signal channel intensities by average normalized control channel

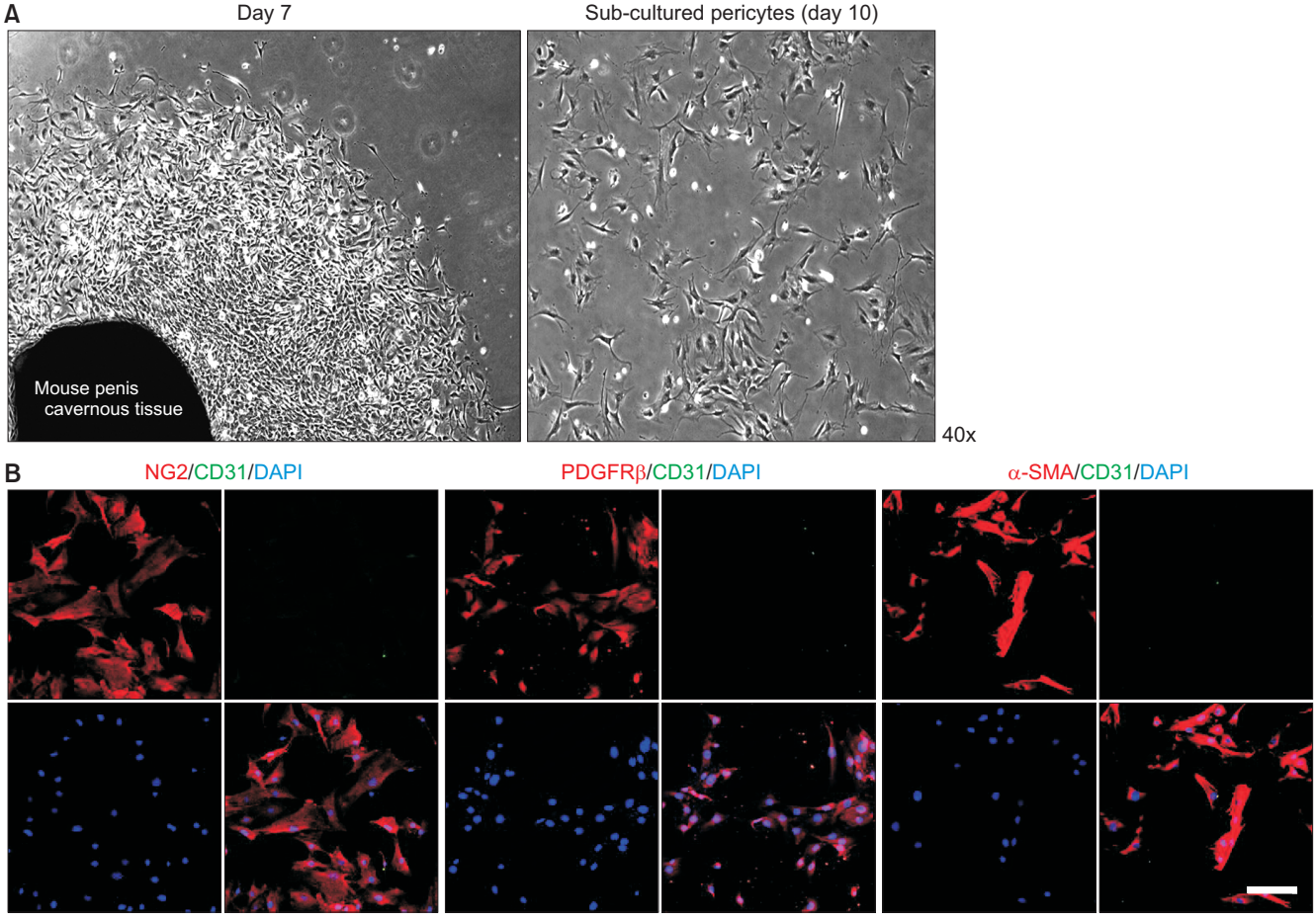

Fig. 1. Isolation and characterization of MCPs. (A) Pericytes were sprouted from mouse cavernous tissues. Photograph showing a representative phage image (screen magnification, 40×, day 7 and day 10). (B) Characterization of MCPs by immunofluorescent staining using antibodies against pericyte markers (NG2 and PDGFRβ), endothelial cell marker (CD31), and smooth muscle α-actin (SMA, a smooth muscle cell and pericyte marker). Nuclei were labeled with DAPI. Scale bar indicates 50 μm. MCPs, mouse cavernous pericytes; DAPI, 4,6-diamidino-2-phenylindole.

https://doi.org/10.4111/icu.20200272

intensities. Functional gene annotation was performed in accordance with the Gene Ontology Consortium guidelines (http://www.geneontology.org/index) using the GeneSpring-GX 7.3. gene classification based on searches performed by the BioCarta (http://www.biocarta.com/), GenMAPP (http://www.genmapp.org/), DAVID (http://david.abcc.ncifcrf.gov/), and MEDLINE databases (http://www.ncbi.nlm.nih.gov/). cDNA microarray data was deposited in the Gene Expression Omnibus database (www.ncbi.nlm.nih.gov/geo, accession no. GSE146357).

6. RT-PCR

Total RNA was extracted from cultured cells using TRIzol (15596026; Invitrogen, Carlsbad, CA, USA), as previously described [5]. RT was performed using 1 μg of RNA in 20 μL of reaction buffer containing oligo dT primer and AccuPower RT Premix kit (140620111L; Bioneer Inc., Daejeon, Korea). PCR was performed with AccuPower PCR Premix kit (2001211A, Bioneer Inc.) and denaturation at 94℃ for 30 seconds and annealing at 60℃ for 30 seconds in a DNA Engine Tetrad Peltier Thermal Cycler. To analyze PCR products, 10-μL aliquots were electrophoresed on 1% agarose gels and detected under ultraviolet light. GAPDH was used as an internal control.

7. Histological examinations

Normal and diabetic mouse cavernous tissues were harvested and fixed in 4% paraformaldehyde overnight at 4℃. Frozen tissue sections (12-μm) were incubated with antibodies for Hebp1 (NBP2-14977; Novus Biologicals, Littleton, CO, USA; 1:100) and PDGFRβ (SC-1627; Santa Cruz Biotechnology; 1:50). After washing 3 times with PBS, sections were incubated with Rabbit DyLight 550 secondary antibody (Abcam, Cambridge, UK; 1:200), Goat Alexa Fluor 488 secondary antibody (Abcam, 1:200), or DAPI (Vector Laboratories, Inc.) for 2 hours at room temperature. Signals were visualized and digital images obtained with a confocal microscope (Nanoscope Systems).

8. Western blot

Cavernous tissues were harvested using RIPA buffer (89900, Sigma-Aldrich). Equal amounts of protein (30 μg per lane) were electrophoresed on 12% sodium dodecylsulfate-polyacrylamide gels. Proteins were then transferred to polyvinylidene fluoride membranes, which were blocked with 5% nonfat dried milk for 1 hour at room temperature. Membranes were then incubated at 4℃ overnight with primary antibodies for *Hebp1* (NBP2-14977; Novus Biologicals; 1:500) and β-actin antibody (Abcam, 1:6000), and subsequently with secondary antibody, such as horseradish peroxidase-conjugated goat anti-rabbit IgG (ab6721, Abcam) and goat anti-mouse IgG (AP308P, Millipore). The signals were visualized using an enhanced chemiluminescence (EBP-1073; Amersham Pharmacia Biotech, Chicago, IL, USA) detection system, and results were quantified by densitometry.

Digital images and PCR and densitometry results were processed using an image analyzer system (Image J 1.34; National Institutes of Health [NIH], Bethesda, MD, USA; http://rsbweb.nih.gov/ij/).

9. Statistical analysis

Statistical analysis was performed using the Mann–Whitney U test. Results are presented as mean±standard error, and statistical significance was accepted for p-val-

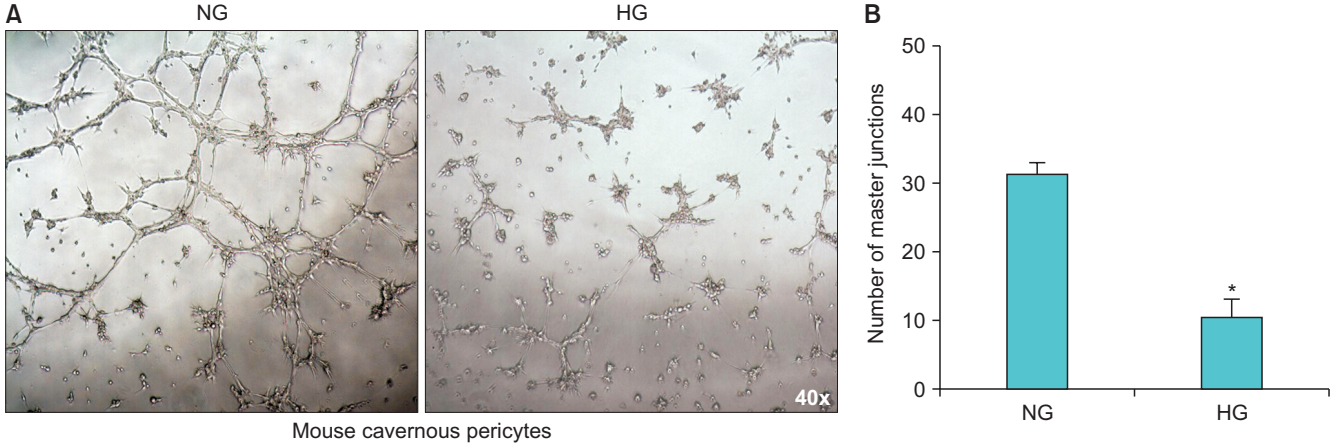

Fig. 2. Reduced tube formation in MCPs exposed to the HG condition. (A) MCPs were exposed to NG or HG conditions for 3 days. Tube formation assays were performed on Matrigel in 96-well dishes. Phase images of MCPs were taken 16 hours after plating (screen magnification, 40×). (B) Bars represent mean numbers of master junctions (±standard error) as determined by four separate experiments. *p<0.001 versus the NG group. NG, normal-glucose; HG, high-glucose; MCPs, mouse cavernous pericytes.

ues<0.05.

RESULTS

1. Isolation and characterization of MCPs

Representative images of sprouted cells at day 7 and passage 1 are shown in Fig. 1A. Cells were cultured until more than 90% confluent (passage 1, about 10 days), and only sprouting cells were used for subsequent studies. MCPs showed finger-like extensions resembling those of normal vascular pericytes [10,17]. Immunofluorescent staining of sprouted cells showed high positive staining for NG2 (a pericyte marker), PDGFRβ (a pericyte marker), and α-SMA (a pericyte and smooth muscle cell marker) but not for CD31 (an

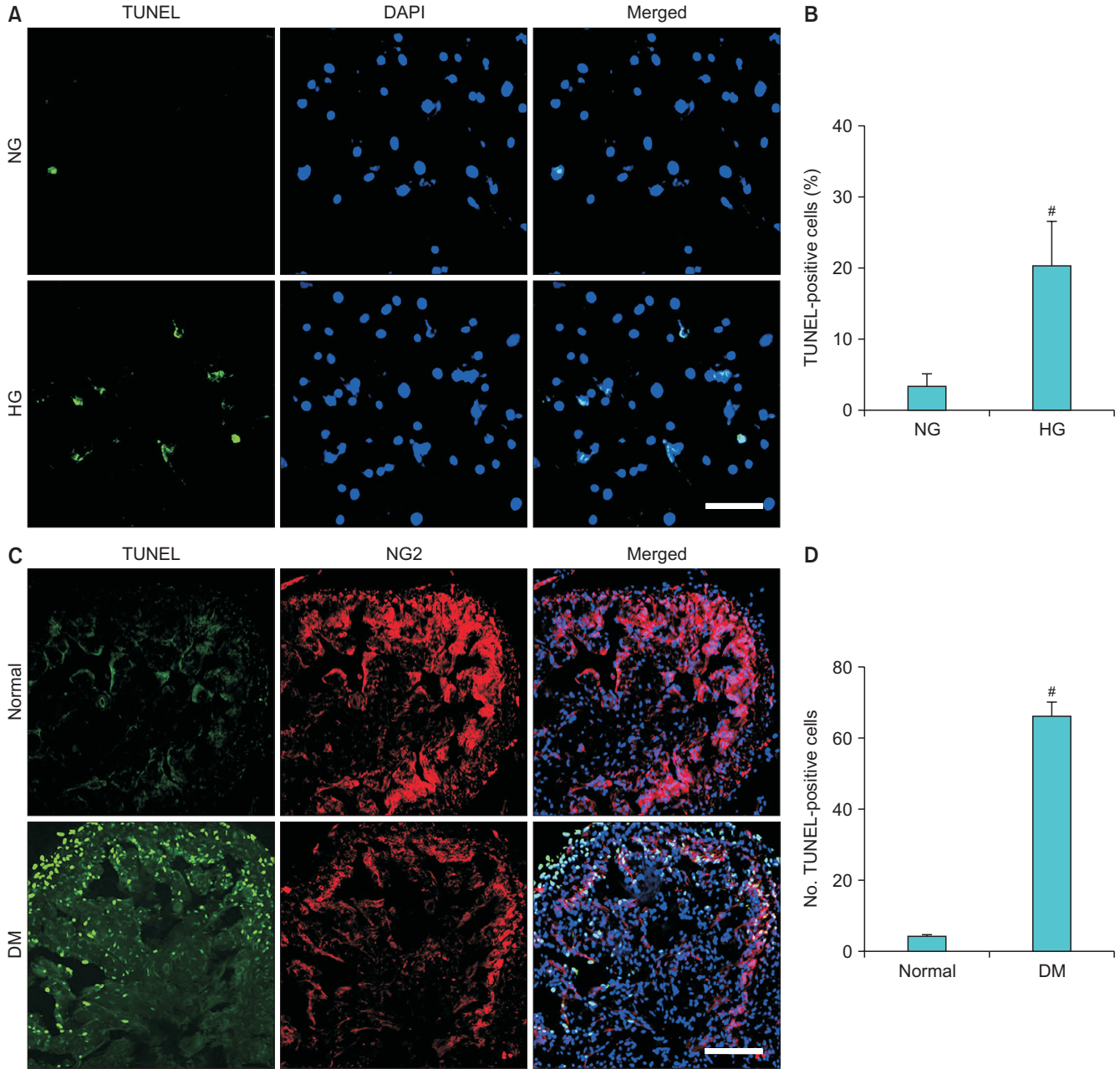

Fig. 3. Increased apoptosis in MCPs under HG and diabetic conditions. (A) MCPs were exposed to NG or HG conditions for 3 days. TUNEL (green) assay in MCPs exposed to NG or HG conditions for 3 days. Nuclei were labeled with DAPI (blue). Scale bar=50 μm. (B) Percentages of apoptotic MCPs per field (screen magnification, 40×). Bars represent the mean values (±standard error) of four separate experiments. #p<0.01 versus the NG group. (C) TUNEL (green) assay and NG2 (a pericyte marker, red) double staining in normal and STZ-induced diabetic mice. Nuclei were labeled with DAPI (blue). Scale bar=50 μm. (D) Number of TUNEL-positive apoptotic MCPs. Bars represent the mean values (±standard error) from 4 mice per group. #p<0.01 versus the normal group. DAPI, 4,6-diamidino-2-phenylindole; TUNEL, terminal deoxynucleotidyl transferase-mediated deoxyuridine triphosphate nick end labeling; NG, normal-glucose; HG, high-glucose; DM, diabetes mellitus; MCPs, mouse cavernous pericytes.

https://doi.org/10.4111/icu.20200272

endothelial cell marker) (Fig. 1B).

2. Reduced tube formation in MCPs exposed to the HG condition

To assess whether MCPs are capable of forming well-organized capillary-like structures and to examine the effects of the NG or HG condition on tube formation, we performed a tube formation assay *in vitro*. After 16 hours, MCPs exposed to the NG condition formed tube-like structures (master junctions), whereas the number of master junctions was significantly less for MCPs exposed to the HG condition (Fig. 2).

3. Increased cell apoptosis in MCPs exposed to the HG condition

To determine the effect of the HG condition on MCPs, we used TUNEL assays to evaluate apoptosis in cells exposed to the NG or HG condition. The results obtained showed that the percentage of apoptotic cells was higher in the MCPs exposed to the HG condition (Fig. 3A, B). In addition, we also evaluated the apoptosis of MCPs through TUNEL assay and NG2 double staining in normal and STZ-induced diabetic mice. The results revealed that the number of apoptotic MCPs significantly increased in STZ-induced diabetic mice compared with normal groups (Fig. 3C, D).

4. Overview of gene expression in the NG versus HG condition

To evaluate the effect of the HG condition on the MCP gene expression profile, two gene libraries from the NG and HG groups (n=3 pooled samples per group) were constructed. In total, 55,681 genes were detected by microarray assay in both libraries. A total of 2,523 significant expressional changes were detected and classified into 15 gene ontology

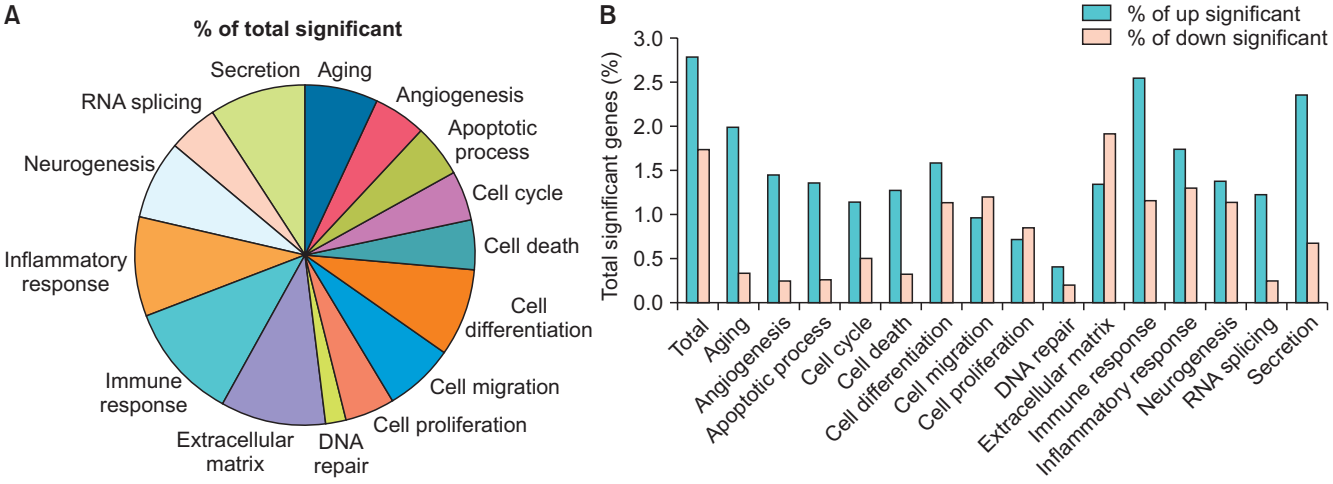

C Significant criteria: 2 fold

PC HG/ PC normal	Total	Aging	Angiogenesis	Apoptotic process	Cell cycle	Cell death	Cell differentiation	Cell migration	Cell proliferation	DNA repair	Extracellular matrix	Immune response	Inflammatory response	Neurogenesis	RNA splicing	Secretion
Gene number	55,681	302	413	1,174	1,407	1,257	4,143	832	702	489	521	861	459	1,746	408	593
% of total	100.0	0.5	0.7	2.1	2.5	2.3	7.4	1.5	1.3	0.9	0.9	1.5	0.8	3.1	0.7	1.1
Up significant	1,551	6	6	16	16	16	66	8	5	2	7	22	8	24	5	14
% of up significant	2.8	2.0	1.5	1.4	1.1	1.3	1.6	1.0	0.7	0.4	1.3	2.6	1.7	1.4	1.2	2.4
Down significant	972	1	1	3	7	4	47	10	6	1	10	10	6	20	1	4
% of down significant	1.7	0.3	0.2	0.3	0.5	0.3	1.1	1.2	0.9	0.2	1.9	1.2	1.3	1.1	0.2	0.7
Total significant	**2,523**	**7**	**7**	**19**	**23**	**20**	**113**	**18**	**11**	**3**	**17**	**32**	**14**	**44**	**6**	**18**
% of total significant	4.5	2.3	1.7	1.6	1.6	1.6	2.7	2.2	1.6	0.6	3.3	3.7	3.1	2.5	1.5	3.0

Fig. 4. Overview of differentially expressed genes under normal-glucose and high-glucose conditions. (A) Genes with significantly different expressions as determined by microarray analysis were classified into 15 gene ontology (GO) categories. (B, C) Percentages and number of genes showing substantial expressional changes (up- or down-regulated) after the application of more stringent selection criteria (≥2-fold change and raw data expression amount >500) to those genes showing expressional changes. HG, high-glucose.

(GO) categories (Fig. 4A) using ExDEGA software (E-Biogen, Inc.). Only the cell migration, cell proliferation, and extracellular matrix categories showed significantly more genes with decreased than increased expression (Fig. 4B). Details of numbers or percentages of significant expressional changes in these GO categories are summarized in Fig. 4C. Additional screening of significant expressional changes was performed by differentially expressed gene (DEG) analysis by applying two conditions: namely, a fold change of >2.0 and a raw data expression amount >500 in the NG or HG condition. As a result, 23 genes were found to be up-regulated and 9 to be down-regulated under the HG condition (Fig. 5A). Genes showing significant expressional changes are listed in Table 1.

5. Validation of microarray results by RT-PCR

After literature search and analysis of the 32 significantly changed genes, we found 3 genes were related to the heme oxygenase (HO) system, namely, *Hebp1*, *Prtm1*, and *Hmox1*, and these genes were chosen for the validation study. The primers used in this study are listed in Table 2. MCPs were exposed to the NG or HG condition, and total RNA was extracted and subjected to RT-PCR. Only *Hebp1* showed a trend in-line with the microarray results and was expressed at significantly lower levels after exposure to the HG condition as determined by RT-PCR (Fig. 5B, C).

A

Significant gene selection (fold change more than 2 and raw data expression amount more than 500)		
Total	Up-regulated	Down-regulated
32	23	9

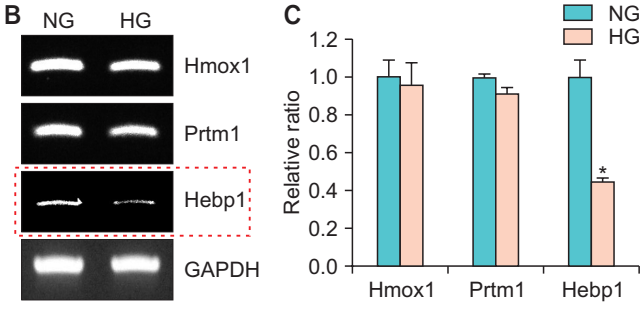

Fig. 5. Further screening of genes showing significant expressional changes and validation by RT-PCR. (A) Differentially expressed genes (DEGs) were selected after applying the two criteria mentioned in the legend of Fig. 3. (B) Three DEGs were evaluated in MCPs exposed to NG or HG conditions for 3 days. (C) Bars represent the mean values (±standard errors) of three separate experiments. *p<0.01 versus the NG group. Expression in the HG group is shown with respect to the corresponding expression in the NG group. NG, normal-glucose; HG, high-glucose; DEGs, differentially expressed genes; MCPs, mouse cavernous pericytes.

6. Decreased expression of Hebp1 in the cavernous tissues of diabetic mice

Double staining of mouse cavernous tissues with antibodies to Hebp1 and PDGFRβ showed that Hebp1 was most expressed in pericytes and that the expression of Hebp1 protein in pericytes was significantly lower in the tissues of diabetic mice (Fig. 6A–C). The fasting and postprandial blood glucose concentrations in STZ-induced diabetic mice were significantly higher than in control mice, and body weight was decreased in STZ-induced diabetic mice. The physiologic and metabolic parameters of normal and diabetic mice are shown in Table 3. The results of the Western blot analysis concurred with the immunofluorescent staining results (Fig. 6D, E).

DISCUSSION

Pericyte dysfunction has recently been reported in diabetes-induced ED [11]. However, the role played by pericytes in diabetic ED has not been determined. To our knowledge, this is the first study to provide global gene expression data on MCPs exposed to NG and HG conditions. In the present study, we performed global microarray analysis to access gene expression profiles and identify the underlying roles of pericytes in diabetes-induced ED. The significantly different gene expression profiles of MCPs cultured under HG and NG conditions appear to support the suggestion made in a recent study that pericyte dysfunction is responsible for diabetes-induced ED.

MCP dysfunction under NG and HG conditions has been well characterized [18]. Therefore, we prepared primary cultures of MCPs from mouse cavernosum tissues and exposed them to glucose conditions mimicking those of diabetes-induced angiopathy. Several studies have demonstrated that endothelial tube formation plays an important role in vascular formation. However, the group of Bagley et al. [18] showed that pericytes wrap around the endothelial cells and also have tube formation properties in the process of vasculogenesis. In addition, we also found that MCPs can form linear networks like endothelial cells [19-21]. In the present study, we found that MCPs formed more substantial tube-like structures under the NG condition, and that rates of MCP apoptosis were greater under the HG condition. These observations indicate that MCP dysfunction may adversely affect angiogenesis and critically influence vascular formation and development.

To identify potential target genes for diabetes-induced

https://doi.org/10.4111/icu.20200272

Table 1. Summary of genes showing a significant difference in expression (fold change of >2, expression >500 in NG or HG) in MCPs exposed to the NG and HG conditions

Gene symbol	PC HG/PC normal	PC HG (raw)	PC normal (raw)	Gene bank accession No.	Description
Tcp10b	0.01	5.39	573.94	NM_009341	T-complex protein 10b (Tcp10b)
Pkhd1l1	0.01	5.51	541.99	NM_138674	Polycystic kidney and hepatic disease 1-like 1 (Pkhd1l1)
Olfr390	0.02	8.12	562.80	NM_146347	Olfactory receptor 390 (Olfr390)
Mdfi	0.29	504.81	1,978.66	NM_001109973	MyoD family inhibitor (Mdfi), transcript variant 2
Taf15	0.43	587.40	1,578.78	NM_027427	TATA box binding protein (TBP)-associated factor (Taf15)
Prr7	0.44	1,186.33	3,090.27	NM_001030296	Proline rich 7 (synaptic) (Prr7)
Plcl2	0.45	324.71	826.26	NM_013880	Phospholipase C-like 2 (Plcl2)
Lrrcc1	0.47	490.42	1,200.19	NM_028915	Leucine rich repeat and coiled-coil domain containing 1 (Lrrcc1)
Hebp1	0.49	2,335.51	5,419.54	NM_013546	Heme binding protein 1 (Hebp1)
Eml2	2.12	575.48	310.52	NM_028153	Echinoderm microtubule associated protein like 2 (Eml2), transcript variant 1
U2af1	2.14	1,548.88	826.41	NM_024187	U2 small nuclear ribonucleoprotein auxiliary factor (U2AF) 1
Trio	2.18	756.92	397.54	NM_001081302	Triple functional domain (PTPRF interacting) (Trio)
Zfp955b	2.22	2,134.97	1,099.86	NM_001142957	Zinc finger protein 955B (Zfp955b)
Lamtor2	2.30	21,770.68	10,826.02	NM_031248	Late endosomal/lysosomal adaptor, MAPK and MTOR activator 2 (Lamtor2)
Prmt1	2.30	9,290.85	4,617.97	NM_019830	Protein arginine N-methyltransferase 1 (Prmt1), transcript variant 1
Eif3j	2.33	6,260.23	3,075.20	NM_144545	Eukaryotic translation initiation factor 3, subunit J (Eif3j)
Tnpo2	2.46	2,286.69	1,061.68	NM_145390	Transportin 2 (importin 3, karyopherin beta 2b) (Tnpo2), transcript variant 1
Wbscr27	2.59	652.29	288.58	NM_024479	Williams Beuren syndrome chromosome region 27 (Wbscr27)
Il11	2.66	979.89	420.96	NM_008350	Interleukin 11 (Il11)
Tifa	2.67	953.32	409.19	NM_145133	TRAF-interacting protein with forkhead-associated domain (Tifa)
Slco4a1	2.92	1,486.80	582.27	NM_148933	Solute carrier organic anion transporter family, member 4a1 (Slco4a1)
Trim12c	3.00	1,021.87	389.32	NM_001146007	Tripartite motif-containing 12C (Trim12c), transcript variant 1
Tmc6	3.24	916.63	323.94	NM_181321	Transmembrane channel-like gene family 6 (Tmc6), transcript variant 2
Stac3	3.31	655.07	226.64	NM_181321	SH3 and cysteine rich domain 3 (Stac3)
Epha1	3.56	2,673.09	859.83	NM_023580	Eph receptor A1 (Epha1)
Alg8	4.69	3,217.93	784.99	NM_199035	Asparagine-linked glycosylation 8 homolog
Hmox1	4.87	5,432.15	1,276.39	NM_010442	Heme oxygenase (decycling) 1 (Hmox1)
Fam133b	5.26	1,414.08	307.48	NM_001042501	Family with sequence similarity 133, member B (Fam133b)
Ext2	8.45	2,433.16	329.64	NM_010163	Exostoses (multiple) 2 (Ext2)
Ccny	8.91	949.65	121.97	NM_026484	Cyclin Y (Ccny)
Klra16	45.60	33,202.81	833.12	NM_013794	Killer cell lectin-like receptor, subfamily A, member 16 (Klra16)

NG, normal-glucose; HG, high-glucose; MCP, mouse cavernous pericyte.

Table 2. Primer list for RT-PCR

Gene	Primer sequence (5' to 3')		Product size (bp)
Hmox1	F: cctcactggcaggaaatcat	R: aaggcggtcttagcctcttc	326
Prtm1	F: tctccaccagtcctgagtcc	R: tattggcataaacgcaacca	339
Hebp1	F: gtgacagacaagccagtgga	R: tgactcatgccttcacaagc	442
GAPDH	F: ccactggcgtcttcaccac	R: cctgcttcaccaccttcttg	501

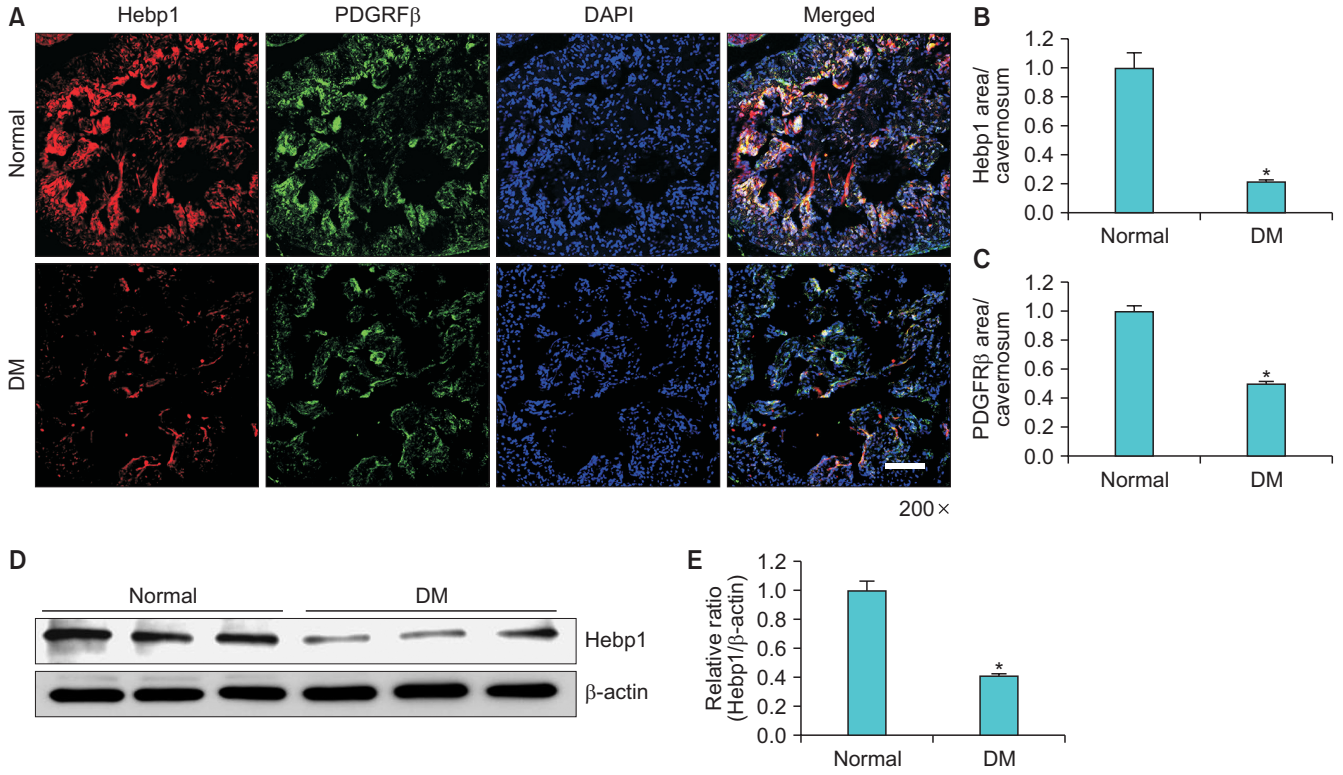

Fig. 6. The down-regulation of Hebp1 under diabetic conditions. (A) Hebp1 (red) and PDGFRβ (a pericyte marker; green) staining in mouse cavernous tissues. Nuclei were labeled with DAPI (blue). Scale bar=100 μm. (B, C) Hebp1 expression and pericyte levels in cavernosum were quantified using Image J software. Bars represent the mean values (±standard errors) of three separate samples. *p<0.01 versus the NG group. (D) Representative western blots for Hebp1 in mouse cavernosum tissues. (E) Normalized band intensities (±standard errors) of three separate samples. *p<0.001 versus the normal group. Expression in the HG group is shown with respect to the corresponding expression in the NG group. PDGFRβ, platelet-derived growth factor receptor-β; DM, diabetes mellitus; NG, normal-glucose; HG, high-glucose.

Table 3. Physiologic and metabolic parameters in normal and STZ-induced diabetic mice

Variable	Normal	STZ-induced diabetic mice
Body weight (g)	33.1±0.8	22.1±0.4*
Fasting glucose (mg/dL)	111.5±4.5	385.7±21.2*
Postprandial glucose (mg/dL)	153.7±3.0	546.7±6.7*

Values are presented as mean±standard error for animals (n=6) per group.
STZ, streptozotocin.
*p<0.01 vs. normal group.

angiopathy, we examined gene expression profiles in HG and NG cultured MCPs and found 1,551 genes were up-regulated (fold change >2) and 972 were down-regulated after exposure to the HG condition. From these genes, we found that the expression of classic pericyte markers (NG2, PDGFRβ) and genes related to vascular stability, such as Angiopoietin1, were significantly decreased in the HG group compared with the NG group, which was consistent with our previous study [10,11,13]. Further screening resulted in the identification of 32 potential target genes. Among these genes, we observed *Hebp1*, *Prtm1*, and *Hmox1*, which are related to the HO system. This system has recently emerged as an important player in diabetes and angiogenesis [22,23]. HO activity is decreased in the aorta of STZ-induced type 1 diabetic rats and in the HG condition *in vitro*, whereas overexpression of the HO-1 gene attenuates endothelial cell sloughing in the STZ animal model [24]. Recently, many studies have also

https://doi.org/10.4111/icu.20200272

shown that increased HO-1 gene expression induces vascular endothelial growth factor (VEGF) and inducible nitric oxide synthase in diabetic animals [25,26]. In addition, Abraham et al. [27] showed VEGF-induced angiogenesis through a mechanism dependent on HO-1 expression. These studies indicated that the HO system plays an important protective role against the harmful effects of hyperglycemia. In the present study, RT-PCR validation showed that only *Hebp1* gene expression was consistent with our microarray results. However, little is known of the function of the HO system in diabetes-induced pericyte dysfunction, and in this study, we found that *Hebp1* expression in cavernosum tissue was significantly lower in DM mice than in normal controls. These results strongly suggest that induction of *Hebp1* expression or activation may be considered one defense against diabetes-induced pericytes dysfunction.

Notably, the present study identifies an interesting therapeutic target for diabetic ED. However, the study has some limitations. First, the glucose conditions did not fully reflect the complexity of diabetes-induced ED and we did not use L-glucose as an osmolality control. Second, we used three pooled samples for each group in the microarray analysis, but we did not perform a separate analysis for each group. Third, we only evaluated genes related to the HO system, and thus, several other genes that showed significant expression changes remain to be validated. Further study on the detailed functions of *Hebp1*, such as overexpression of *Hebp1* in diabetic animals would importantly contribute to our understanding of the mechanisms responsible for diabetes-induced ED.

CONCLUSIONS

This study provides profiles of DEGs in MCPs exposed to normal and high glucose concentrations and suggests that decreased *Hebp1* expression may be a potential biomarker for diabetes-induced ED.

CONFLICTS OF INTEREST

The authors have nothing to disclose.

ACKNOWLEDGMENTS

This research was supported by grants of the National Natural Science Foundation of China (Hai-Rong Jin, 81871156; Jitao Wu, 81870525), by a National Research Foundation of Korea (NRF) grant (Jun-Kyu Suh, 2018R1A2B2002955), and by a Medical Research Center Grant (Ji-Kan Ryu, 2014R1A5A2009392) funded by the Korean government (Ministry of Science, ICT and Future Planning).

AUTHORS' CONTRIBUTIONS

Research conception and design: Guo Nan Yin and Jitao Wu. Data acquisition: Guo Nan Yin, Jitao Wu, Yuanshan Cui, Chunhua Lin, Lei Shi, and Zhen-Li Gao. Statistical analysis: Guo Nan Yin. Data analysis and interpretation: Guo Nan Yin and Jitao Wu. Drafting of the manuscript: Guo Nan Yin, Jitao Wu, and Jun-Kyu Suh. Critical revision of the manuscript: Ji-Kan Ryu and Hai-Rong Jin. Obtaining funding: Jitao Wu, Ji-Kan Ryu, and Hai-Rong Jin. Administrative, technical, or material support: Guo Nan Yin, Jitao Wu, Yuanshan Cui, Chunhua Lin, Lei Shi, and Zhen-Li Gao. Supervision: Ji-Kan Ryu and Hai-Rong Jin. Approval of the final manuscript: All authors.

REFERENCES

1. Jin HR, Kim WJ, Song JS, Choi MJ, Piao S, Shin SH, et al. Functional and morphologic characterizations of the diabetic mouse corpus cavernosum: comparison of a multiple low-dose and a single high-dose streptozotocin protocols. J Sex Med 2009;6:3289-304.
2. Musicki B, Burnett AL. Endothelial dysfunction in diabetic erectile dysfunction. Int J Impot Res 2007;19:129-38.
3. Birbrair A, Zhang T, Wang ZM, Messi ML, Mintz A, Delbono O. Pericytes at the intersection between tissue regeneration and pathology. Clin Sci 2015;128:81-93.
4. Díaz-Flores L, Gutiérrez R, Varela H, Rancel N, Valladares F. Microvascular pericytes: a review of their morphological and functional characteristics. Histol Histopathol 1991;6:269-86.
5. Winkler EA, Bell RD, Zlokovic BV. Central nervous system pericytes in health and disease. Nat Neurosci 2011;14:1398-405.
6. Armulik A, Abramsson A, Betsholtz C. Endothelial/pericyte interactions. Circ Res 2005;97:512-23.
7. Armulik A, Genové G, Betsholtz C. Pericytes: developmental, physiological, and pathological perspectives, problems, and promises. Dev Cell 2011;21:193-215.
8. von Tell D, Armulik A, Betsholtz C. Pericytes and vascular stability. Exp Cell Res 2006;312:623-9.
9. Fu D, Wu M, Zhang J, Du M, Yang S, Hammad SM, et al. Mechanisms of modified LDL-induced pericyte loss and retinal injury in diabetic retinopathy. Diabetologia 2012;55:3128-40.
10. Yin GN, Jin HR, Choi MJ, Limanjaya A, Ghatak K, Minh NN,

et al. Pericyte-derived Dickkopf2 regenerates damaged penile neurovasculature through an angiopoietin-1-Tie2 pathway. Diabetes 2018;67:1149-61.

11. Yin GN, Park SH, Song KM, Limanjaya A, Ghatak K, Minh NN, et al. Establishment of in vitro model of erectile dysfunction for the study of high-glucose-induced angiopathy and neuropathy. Andrology 2017;5:327-35.
12. Neng L, Zhang W, Hassan A, Zemla M, Kachelmeier A, Fridberger A, et al. Isolation and culture of endothelial cells, pericytes and perivascular resident macrophage-like melanocytes from the young mouse ear. Nat Protoc 2013;8:709-20.
13. Yin GN, Das ND, Choi MJ, Song KM, Kwon MH, Ock J, et al. The pericyte as a cellular regulator of penile erection and a novel therapeutic target for erectile dysfunction. Sci Rep 2015;5:10891.
14. Li L, Sawamura T, Renier G. Glucose enhances endothelial LOX-1 expression: role for LOX-1 in glucose-induced human monocyte adhesion to endothelium. Diabetes 2003;52:1843-50.
15. Poczatek MH, Hugo C, Darley-Usmar V, Murphy-Ullrich JE. Glucose stimulation of transforming growth factor-beta bioactivity in mesangial cells is mediated by thrombospondin-1. Am J Pathol 2000;157:1353-63.
16. Detaille D, Guigas B, Chauvin C, Batandier C, Fontaine E, Wiernsperger N, et al. Metformin prevents high-glucose-induced endothelial cell death through a mitochondrial permeability transition-dependent process. Diabetes 2005;54:2179-87.
17. Nguyen NM, Song KM, Choi MJ, Ghatak K, Kwon MH, Ock J, et al. Inhibition of proNGF and $p75^{NTR}$ pathway restores erectile function through dual angiogenic and neurotrophic effects in the diabetic mouse. J Sex Med 2019;16:351-64.
18. Bagley RG, Weber W, Rouleau C, Teicher BA. Pericytes and endothelial precursor cells: cellular interactions and contributions to malignancy. Cancer Res 2005;65:9741-50.
19. Ndisang JF. Role of heme oxygenase in inflammation, insulin-signalling, diabetes and obesity. Mediators Inflamm 2010;2010:359732.
20. Moreno-Navarrete JM, Ortega F, Rodríguez A, Latorre J, Becerril S, Sabater-Masdeu M, et al. HMOX1 as a marker of iron excess-induced adipose tissue dysfunction, affecting glucose uptake and respiratory capacity in human adipocytes. Diabetologia 2017;60:915-26.
21. Tiwari S, Ndisang JF. The heme oxygenase system and type-1 diabetes. Curr Pharm Des 2014;20:1328-37.
22. Quan S, Kaminski PM, Yang L, Morita T, Inaba M, Ikehara S, et al. Heme oxygenase-1 prevents superoxide anion-associated endothelial cell sloughing in diabetic rats. Biochem Biophys Res Commun 2004;315:509-16.
23. Abraham NG, Rezzani R, Rodella L, Kruger A, Taller D, Li Volti G, et al. Overexpression of human heme oxygenase-1 attenuates endothelial cell sloughing in experimental diabetes. Am J Physiol Heart Circ Physiol 2004;287:H2468-77.
24. Ahmad M, Turkseven S, Mingone CJ, Gupte SA, Wolin MS, Abraham NG. Heme oxygenase-1 gene expression increases vascular relaxation and decreases inducible nitric oxide synthase in diabetic rats. Cell Mol Biol (Noisy-le-grand) 2005;51:371-6.
25. Bussolati B, Mason JC. Dual role of VEGF-induced heme-oxygenase-1 in angiogenesis. Antioxid Redox Signal 2006;8:1153-63.
26. Bussolati B, Ahmed A, Pemberton H, Landis RC, Di Carlo F, Haskard DO, et al. Bifunctional role for VEGF-induced heme oxygenase-1 in vivo: induction of angiogenesis and inhibition of leukocytic infiltration. Blood 2004;103:761-6.
27. Abraham NG, Tsenovoy PL, McClung J, Drummond GS. Heme oxygenase: a target gene for anti-diabetic and obesity. Curr Pharm Des 2008;14:412-21.

https://doi.org/10.4111/icu.20200272